4 Cerebral Blood Flow Measurement with Oxygen-15 Water Positron Emission Tomography

Vilia Zeisig, Marianne Patt, Georg Becker, Johannes Boltze, Osama Sabri, and Henryk Barthel

Contents

Abstract

The human brain receives approximately 15 % of the cardiac output and therefore is the most demanding organ in respect to blood flow supply. This fact emphasizes the importance of perfusion as a key factor in a variety of cerebrovascular

V. Zeisig (✉) • M. Patt, PhD • G. Becker, PhD • O. Sabri, MD, PhD • H. Barthel, MD, PhD
Department of Nuclear Medicine, University Hospital Leipzig, University of Leipzig, Liebigstrasse 18, Leipzig 04103, Germany
e-mail: vilia.zeisig@medizin.uni-leipzig.de; marianne.patt@medizin.uni-leipzig.de; georg.becker@medizin.uni-leipzig.de; osama.sabri@medizin.uni-leipzig.de; henryk.barthel@medizin.uni-leipzig.de

J. Boltze, MD, PhD
Department of Cell Therapy, Ischemia Research Unit, Fraunhofer Institute for Cell Therapy and Immunology, Perlickstraße 1, Leipzig 04103, Germany

Translational Centre for Regenerative Medicine, University of Leipzig, Philipp-Rosenthal-Str. 55, 04103 Leipzig, Germany
e-mail: johannes.boltze@izi.fraunhofer.de

R.A.J.O. Dierckx et al. (eds.), *PET and SPECT of Neurobiological Systems*,
DOI 10.1007/978-3-642-42014-6_4, © Springer-Verlag Berlin Heidelberg 2014

and other diseases including stroke, migraine, and brain tumors. Today, numerous imaging techniques are able to visualize brain perfusion, but only few of them provide quantitative information. In the field of modern in vivo imaging techniques, positron emission tomography (PET) is considered to be the gold standard to give reliable results about major aspects of cerebral physiology. $[^{15}O]H_2O$ allows for quantitative cerebral blood flow (CBF) measurement within a few minutes, and subsequent ^{15}O imaging can provide precise information on oxygen metabolism like cerebral oxygen metabolism and oxygen extraction fraction. As a result, PET has become an extremely useful research tool for defining cerebral blood flow and physiology. However, complex methodological logistics and a limited availability of the imaging system hamper the widespread use of CBF PET in clinical routine. The chapter aims at summarizing the radiosynthesis, data acquisition, and analysis, as well as major preclinical and clinical applications of $[^{15}O]H_2O$ PET.

Abbreviations

$c_a(t)$	Arterial input function (arterial activity concentration over time)
CBF	Cerebral blood flow
CBV	Cerebral blood volume
$CMRO_2$	Cerebral metabolic rate of oxygen
CT	Computed tomography
$c_v(t)$	Activity concentration in venous blood over time
f_a	Arterial blood flow
GBq	Gigabecquerel
GM	Gray matter
IAP	Iodoantipyrine
iNO	Inhaled nitric oxide
k	Washout-constant
kBq	Kilobecquerel
MBq	Megabecquerel
MRI	Magnetic resonance imaging
NO	Nitric oxide
OEF	Oxygen extraction fraction
PET	Positron emission tomography
rCBF	Regional cerebral blood flow
ROI	Region of interest
S/N	Signal-to-noise
SPECT	Single-photon emission computed tomography
TSE	Turbo spin echo
V_d	Partition coefficient
V_{tissue}	Tissue volume
WM	White matter
Xe	Xenon

4.1 Introduction

Although the adult human brain assumes only about 2 % of the total body weight, it receives nearly 15 % of the resting cardiac output and 20 % of the total body oxygen consumption. This high metabolic rate reveals the need to ensure a constant delivery of oxygen and energy-providing substrates at the capillary level and to remove the waste products of metabolism. Owing to a complex autoregulatory mechanism, the cerebral perfusion is maintained relatively constant over a wider range of mean arterial pressures. A complete interruption of brain–blood supply, however, leads immediately to neuronal impairments because of the limited availability of nutrition and energy reserves in the brain. Hence, perfusion parameters are important key factors involved in major cerebrovascular and other brain diseases. Important information about cerebral characteristics is given by measurement of the cerebral blood flow (CBF) which describes the rate of blood delivery to the brain parenchyma. Traditionally, the respective literature reports CBF units in ml blood/100 g of tissue per minute. Other authors use ml instead of gram tissue to describe the volumetric character especially with imaging techniques. Due to the fact that 1 g of brain tissue nearly corresponds to 1 ml, both values can be more or less used interchangeably.

Global average CBF values in middle-aged healthy human subjects are around 55 ml/100 g/min (Kety and Schmidt 1945). However, CBF values vary regionally: In cortical gray matter, the CBF is 60–100 ml/100 g/min (Slosman et al. 2001; Sokoloff et al. 1957) and around 20 ml/100 g/min for white matter (Law et al. 2000). It has been demonstrated that neuronal activity as well as CBF is closely coupled to brain metabolism (Pantano et al. 1984; Roy and Sherrington 1890). This may explain the generally higher blood flow in younger subjects which is typically exceeding values that are 50–85 % higher than those of adults (age: 6–7 years, Chiron et al. 1992). This age dependency of CBF is probably caused, at least in parts, by an age effect on the gray-to-white matter ratio. Additionally, a decline of CBF with age is described (Brody 1955).

Kety and Schmidt (1945) were the first who introduced a method for quantitative CBF measurement in the unanesthetized human. This method is based on the Fick principle. During the inhalation of the freely diffusible nitrous oxide, the brain perfusion was calculated by measuring the amount of gas removed from the blood by the brain per minute and dividing this by the arteriovenous difference of N_2O. This method was an important step to study brain function in humans and has contributed fundamentally to our understanding of physiological and pathological cerebral processes. However, this first technique lacked the possibility to measure CBF in different brain subregions. This limitation has led to further developments in perfusion imaging techniques. As important examples, radioactive agents such as ^{133}Xe and ^{85}Kr were later used to measure their washout with external radiation detectors (Lassen and Ingvar 1961; Veall and Mallett 1967; Bruce et al. 1973; Obrist et al. 1975). Today, a wide variety of brain perfusion imaging techniques is available for preclinical and clinical research settings as well as clinical routine applications. CBF measurement using positron emission tomography (PET) became available in the 1970s, followed by other in vivo imaging techniques, like single-photon emission computed tomography (SPECT), magnetic resonance imaging (MRI), and transmission computed tomography (CT), to obtain CBF readouts (Hoeffner 2005). This chapter will focus on CBF PET with [^{15}O]H_2O as this represents the gold standard technique for in vivo CBF measurements (Carroll et al. 2002; Hoeffner 2005). One possible application for its usage is studying CBF in brain activation studies to localize brain segments involved in processing certain tasks. More important today, however, is the diagnostic potential of CBF PET imaging mainly in cerebrovascular disorders and oncology. Hence alterations of cerebral perfusion can theoretically be detected by quantitative CBF measurement leading to optimal therapy and providing estimates of the potentially salvable part of the affected brain.

4.2 Radiochemistry of [^{15}O]H_2O

Oxygen-15 can be produced by different nuclear reactions using both high- and low-energy protons as well as deuterons as projectiles. The ^{14}N(d, n)^{15}O nuclear reaction is the most efficient and economic production pathway and is therefore applied most frequently. For cyclotrons that do not have the possibility of accelerating deuterons, either the ^{15}N(p, n)^{15}O (Powell and O'Neil 2006) for low-energy protons (>3.7 MeV) or the ^{16}O(p, pn)^{15}O (Beaver et al. 1976; Krohn et al. 1986) for high-energy protons (>16.6 MeV) nuclear reactions can be used as an alternative.

Two methods are available for conversion of the ^{15}O to [^{15}O]H_2O, the in-target production method and the out-of-target external conversion method. In case of the in-target production method, [^{15}O]H_2O is produced by either addition of small amounts of hydrogen to the target gas or direct irradiation of $H_2{}^{16}O$. For the first approach, the ^{15}N(p, n)^{15}O nuclear reaction is used (Powell and O'Neil 2006), and the trace amounts of H_2 in the target lead to the formation of [^{15}O]H_2O by radiolytic reactions which can be trapped in a cooled stainless steel loop. The possible radioactive impurities such as $^{11}CH_4$ and $^{13}NH_3$ (resulting from trace amounts of N-14 and O-16 in the target gas) are directed to the exhaust. By heating the loop, [^{15}O]H_2O vapor is released and can be trapped again in a sterile water or saline solution. The major drawbacks are the high costs for enriched $^{15}N_2$ which is used as target material. An alternative approach for [^{15}O]H_2O in-target production is the direct irradiation of $H_2{}^{16}O$ in a liquid target (Mulholland et al. 1990; van Naemen et al. 1996). As mentioned above this method is feasible only with high-energy protons, a restriction that excludes this approach for commonly used cyclotrons in a clinical setting.

As an alternative to the in-target production of [^{15}O]H_2O, external out-of-target tracer production by catalytic conversion of a mixture of H_2 and [^{15}O]O_2 has been demonstrated for all abovementioned nuclear reactions, i.e., ^{16}O(p, pn)^{15}O (Krohn et al. 1986), ^{15}N(p, n)^{15}O (Explora®H_2O module, Siemens Healthcare, Erlangen, Germany), and ^{14}N(d, n)^{15}O (Clark et al. 1987; Clark and Tochon-Danguy 1991; Sajjad et al. 2000). For the ^{14}N(d, n)^{15}O nuclear reaction, N_2 with up to 4 % O_2 is irradiated with deuterons (≈7 MeV). In most cases, Pd is used as the catalyst; however, if the same target is used as well for production of $C^{15}O$, it might be necessary to reduce the amount of O_2 in order to minimize the production of toxic carrier CO. Under these conditions it has been shown that Pt as catalyst is superior (Berridge et al. 1990). The most simple production and application approach consists of an H_2 supply that is connected to the target line via a T connector. The target gas/H_2 mixture (2–10 %, Berridge et al. 1990; Sajjad et al. 2000) is then directed over the heated catalyst (≈170 °C, temperatures up to 450 °C have been reported as well (Berridge et al. 1990)), and the resulting $[^{15}O]H_2O$ vapor is bubbled into a sterile reservoir containing water, saline, or preferably buffer since the catalyst might as well generate trace amounts of ammonia which un-buffered may lead to elevated pH values. The $[^{15}O]H_2O$-containing solution is then drawn up into a syringe and manually applied to the investigated subject. However, due to the relatively high radiation exposure of the medical personnel, it might be worth to automate the injection procedure. In a relatively simple setup, the injection is performed by means of two infusion pumps and a 4-port valve (Sajjad et al. 2000). A more sophisticated method uses a dialysis membrane to enable exchange of $[^{15}O]H_2O$ with sterile water (Clark and Tochon-Danguy 1991) together with an infusion pump and several valves to enable automatic injection. This system is commercially available (Veenstra Instruments, Joure, Netherlands).

4.3 $[^{15}O]H_2O$ Brain PET Data Generation

After a transmission scan for attenuation correction, the emission scan is acquired preferentially in 3D mode and initiated immediately before tracer administration. The tracer is injected as a fast bolus followed by a flush of inert saline solution. The amount of injected tracer in humans typically ranges between 550 and 1,000 MBq for an adult subject, but studies using up to 2.2 GBq were also found in the literature (Heiss et al. 2000).

For the bolus injection method, Kanno et al. (1991) investigated an optimal scan time for $[^{15}O]H_2O$ to improve image quality and signal-to-noise ratios. A minimum scan duration of 90 s was recommended. For most applications, however, scan durations of 2–5 min are chosen. A typical protocol for a 5-min dynamic data acquisition is shown in Table 4.1.

The advantageous short half-life of the tracer (122 s) enables the performance of multiple image acquisition scans in rapid sequence. Inter-scan intervals should, however, not be shorter than 15 min to allow isotope decay. Due to the fast radioactive decay, an on-site cyclotron or linear accelerator for isotope production becomes necessary. Further data analyses generally include the absolute quantification of CBF. For this purpose, the experimental setting implies arterial blood sampling in parallel to the PET acquisition. This is preferentially performed using an automated

Table 4.1 Acquisition protocol for a 5-min PET scan with $[^{15}O]H_2O$

Frame duration[s]	5	10	30
Number of frames	24	12	2

sampling system (e.g., ALLOGG AB blood sampler; Allogg Mariefred, Sweden) with a peripheral artery, e.g., the radial artery. Using such a device, arterial blood samples are continuously drawn at a constant speed with activity measurements for every 0.5 or 1 s. The blood sampler needs to be cross-calibrated to the PET scanner, allowing the decay-corrected blood data to be used as input function for kinetic modeling.

Obtaining arterial blood samples via the placement of an arterial catheter is accepted as the gold standard method for CBF quantification. However, there are some limitations, like invasiveness, complications for the patient, and sensitivity to errors (Hall 1971; Machleder et al. 1972). Aiming to replace the arterial canalization and corresponding input function, alternatives were suggested, like image-derived input functions (Zanotti-Fregonara et al. 2011) and methods without the need of any input function (Lammertsma 1994; Watabe et al. 1996). Another possibility to avoid arterial canalization is the use of arterialized venous blood, which is an often used method also with other PET tracers. With this technique, the hand of the patient or volunteer is heated well above 37 °C to achieve a shunting of arterial blood to the venous system (Wakita et al. 2000). Nevertheless, all alternative techniques have their drawbacks, and the CBF values obtained by them need to be handled with caution.

As for all brain PET tracers, the resulting PET data require a correlation with structural information from MRI (preferably 3D-T1 data). In this regard, the use of combined PET/MRI scanners might improve this situation in the future. Combined PET/MR imaging gives the opportunity for accurate registration and exact correlation of PET functional aspects with anatomical information from MRI. This will result in better image quality because of the comparably lower spatial resolution of PET in contrast to MRI and also shortens imaging times for the patients/anesthetized research animals.

4.4 Kinetic Modeling of CBF

The first method to measure CBF in humans was proposed by Kety and Schmidt in 1945 who utilized nitrous oxide for CBF detection. Later, other tracers like ^{133}Xenon (Veall and Mallett 1967) were applied within this concept which was based on the Fick principle and a single-tissue compartment model. It states that the amount of a metabolically inert and freely diffusible gas that is taken up by a tissue per unit of time is equal to the product of the blood flow through that tissue and the difference between the amount of gas entering it via the arterial blood and the gas leaving in the venous blood.

The single-tissue compartment model describes the behavior of a freely diffusible tracer like [^{15}O]H_2O in tissue as shown in Fig. 4.1 and can be used to determine the local arterial blood flow in the brain (on a region of interest (ROI) or voxel basis). The model consists of two parameters that have to be estimated from the data of a dynamic PET scan ($q(t)$) and from the measured arterial input function $c_a(t)$.

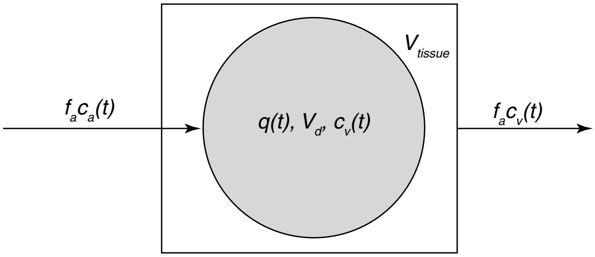

Fig. 4.1 Schematic description of a single-tissue compartment. V_{tissue} is the anatomical tissue volume (1 cm^3), and V_d is the volume of the tissue compartment accessible to the tracer. The products of flow and concentration describe the amount of tracer which enters or leaves the tissue compartment per time unit. Please refer to the main text for further explanation of the other symbols

Assuming that the transport of tracer from the vessel into the tissue compartment is fast (high permeability surface area product) compared to the delivery by the arterial blood flow, the tracer dynamics can be described by a one-tissue compartment model with one input function. The mass balance for the tracer (Fick principle) yields the differential equation

$$\frac{\mathrm{d}q(t)}{\mathrm{d}t} = f_\text{a} c_\text{a}(t) - f_\text{a} c_\text{v}(t) \tag{4.1}$$

where $q(t)$ is the quantity of tracer per unit volume of tissue (kBq cm^{-3}), f_a is the local arterial blood flow per unit volume (ml min^{-1} cm^{-3}), and $c_\text{a}(t)$ and $c_\text{v}(t)$ are the tracer concentrations in arterial and venous blood (kBq ml^{-3}).

The tracer concentration in the venous blood ($c_\text{v}(t)$) is related to the tracer concentration in the tissue space ($q(t)$) through the relative volume of distribution (V_d (ml cm^{-3})) by the Kety–Schmidt assumption:

$$q(t) = V_\text{d} c_\text{v}(t) \tag{4.2}$$

reflecting the assumption that the concentrations in the water spaces of venous blood and tissue are always equilibrated (this assumption is not generally valid, because a diffusion limitation exists for [^{15}O]H_2O at low CBF rates).

From Eqs. (4.1) and (4.2), the differential equation

$$\frac{\mathrm{d}q(t)}{\mathrm{d}t} = f_\text{a} c_\text{a}(t) - kq(t) \tag{4.3}$$

is obtained with the washout constant k (min^{-1}) defined to be

$$k = \frac{f_\text{a}}{V_\text{d}}. \tag{4.4}$$

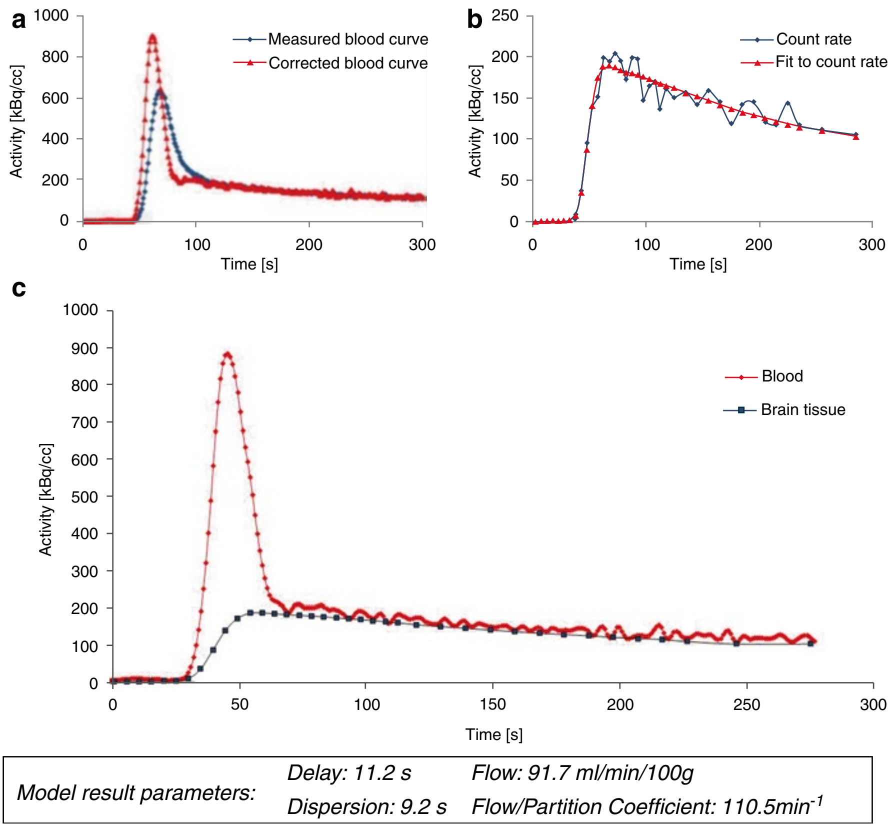

Fig. 4.2 Model parameter estimation. The arterial input function (**a**) and corresponding tissue response in a cortical ROI (**b**) after bolus injection of [^{15}O]H_2O are shown. Blood activity data were determined by taking arterial blood samples with a dedicated sampling device. The input function and tissue response are corrected for tracer arrival times and bolus dispersion. Further kinetic modeling is based on the resulting corrected curves (**c**)

By estimating values of f_a and k, the partition coefficient of the tracer can be calculated for every tissue voxel. An example of parameter estimation for a cortical region of interest based on the arterial input function is shown in Fig. 4.2.

Equation (4.3) has the solution

$$q(t) = f_a e^{-kt} \otimes c_a(t) \tag{4.5}$$

where $\otimes$ describes the convolution of an exponential function with the arterial input function $c_a(t)$:

$$e^{-kt} \otimes c_a(t) = \int_0^t te^{-kt} c_a\left(t - \hat{o}\right) \mathrm{d}\hat{o}. \tag{4.6}$$

The experimental design is further specified in a way that the tissue response, $q(t)$, as well as the arterial, $c_a(t)$, input is measured and thus known for the duration of the experiment. Additionally, $q(0) = 0$.

[^{15}O]H_2O is the most commonly used tracer for brain perfusion imaging and CBF quantification with PET. However, there are some notable restrictions concerning the diffusion limitation of [^{15}O]H_2O. A study of Eichling et al. investigated the cerebral behavior of [^{15}O]H_2O after administration to rhesus monkeys. They found that only about 90 % of the injected tracer freely exchanges with the brain tissue, with even lower rates at higher flow rates. This incomplete first-pass extraction (80–90 % in gray matter structures) resulted in a slightly underestimation of CBF especially in high-flow regions (Eichling et al. 1974; Bolwig and Lassen 1975; Raichle et al. 1983).

In this respect, lipophilic gaseous tracers (like nitrous oxide and xenon) behave superior for CBF measurements as compared with [^{15}O]H_2O.

Further consideration should be done concerning partial volume effect that among others derive from relatively low spatial resolution of typically 6–10 mm in PET. The resulting spread out of signal is a phenomenon that introduces distortion effects in the targeted region and adjacent tissue (Links et al. 1996). The partial volume effect primarily leads to an increased bias for small anatomical structures (like vessels) in the brain (Rousset et al. 1998).

Since the early 1980s, several methods have been described to calculate CBF from PET measurements with [^{15}O]H_2O, including simplified techniques that include parameter fixation, e.g., fixation of the partition coefficient (Watabe et al. 1996). The partition coefficient of [^{15}O]H_2O is a parameter that has been investigated in many studies and varies from 0.77 to 1.05 ml/ml (Herscovitch and Raichle 1985; Iida et al. 1993; Kanno et al. 1991). A good approximation for the whole brain was considered by Herscovitch and Raichle to be 0.9 ml/ml (Herscovitch and Raichle 1985). However, CBF calculation methods with fixed values for V_d are only applicable to identify global blood flow changes. In presence of regional blood flow deficits, CBF calculation results in incorrect values.

4.5 Role of PET for CBF Measurements

4.5.1 General Principles for CBF Measurements

A general distinction must be made between the behaviors of different CBF tracers. One class of techniques utilizes agents which are restricted to the intravascular space and do not interact with the nonvascular space. These can be, in cases of an intact blood–brain barrier, referred to as nondiffusible CBF tracers. Many brain imaging techniques, such as contrast-enhanced MR and CT, use these intravascular tracers to calculate CBF on the basis of the indicator dilution theory (Meier and Zierler 1954; Zierler 1962). In contrast, a direct tracer exchange from the arterial vascularity to the parenchyma occurs in case of freely diffusible CBF tracers and enables to give a direct measurement of parenchymal blood flow, as originally described by Kety (1951). This concept is utilized, for example, with [^{15}O]H_2O PET, Xenon–CT, and Xenon SPECT. Some basic characteristics appear to be necessary for a useful CBF measurement method: Ideally, the incorporated indicator should be early and completely mixed with blood and must stay identifiable for position and concentration in time of image acquisition. Further, the indicator should be metabolically inert and rapidly eliminated.

4.5.2 Advantages and Disadvantages of Perfusion Imaging Methods

Various modalities have been developed to obtain hemodynamic parameters in research and clinical settings. These include the older ^{133}Xe inhalation method, PET, SPECT, X-ray computed tomography methods, and several MRI techniques. However, each technique has its own advantages and drawbacks. It depends on the study subject and the targeted question which method to choose appropriately. A review from Wintermark et al. (2005) gives a comparative overview about current brain perfusion measurement techniques and their clinical relevance. At this point, a brief overview is given on the role of [^{15}O]H_2O PET in this context.

4.5.2.1 Nuclear Medicine Methods

CBF can be measured after incorporation of radioactive agents which are detected outside the investigated subject with dedicated scintillation detectors. Based on this principle, tracers like [^{99m}Tc]HMPAO or [^{99m}Tc]ECD and ^{133}Xe were commonly used for CBF measurements with SPECT (Barthel et al. 2001; Lass et al. 1998; Sakai et al. 1987). In comparison to the coincidence method in PET imaging, the detection of single photons is less sensitive. SPECT imaging with [^{99m}Tc]HMPAO or [^{99m}Tc]ECD only allows for semiquantitative CBF estimation (Markus 2004). In contrast, the ^{133}Xe SPECT method relies on the Kety–Schmidt model (Kety and Schmidt 1945) and is considered to give quantitative measures of CBF (Wintermark et al. 2005). In several studies, however, a systematic CBF overestimation was reported in low-flow areas, as well as an underestimation of cortical CBF (Matsuda et al. 1996; Skyhøj Olsen et al. 1981).

However, the coincidence PET technique is commonly accepted to be the reference standard for CBF imaging. With PET, the tissue perfusion can be directly measured by using the diffusible radiotracer [^{15}O]H_2O. This method is well validated and combines several favorable properties. The tracer is easy to produce, and the fast acquisition time permits repetitive measurements with whole brain coverage. Additionally, the major advantage of CBF measurement with PET is the high accuracy for assessing quantitative parameter maps as well as a high reproducibility (Carroll et al. 2002; Matthew et al. 1993).

Additionally, PET imaging with ^{15}O-labeled compounds is of special interest for studying cerebrovascular diseases and if a comprehensive view on brain hemodynamic is demanded. In addition to the determination of CBF with [^{15}O]H_2O, a successive ^{15}O inhalation allows for quantitative determination of essential parameters of hemodynamics and energy metabolism like oxygen consumption (cerebral metabolic rate of oxygen; $CMRO_2$) and oxygen extraction fraction (OEF) (Frackowiak et al. 1980; Ibaraki et al. 2004). Further, because of its binding to hemoglobin in red blood cells (Martin et al. 1987), radiolabeled CO is used as an intravascular tracer to measure the cerebral blood volume (CBV). Compared to other modalities, PET is the only technique which is able to gain all of these different functional parameters noninvasively and in 3D for the entire brain, a fact which allowed PET imaging to become the gold standard method in the field of brain circulation physiology and pathophysiology imaging (Hoeffner 2005).

In comparison to SPECT, which is widely accessible and a routine perfusion imaging tool, PET imaging is technically more demanding and its availability is limited by complex logistics. Not only a PET scanner, but also the constant access to a cyclotron producing the radiopharmaceutical online is required, a fact limiting the application of the method especially in emergency settings. A further restriction occurs in patients who will receive a thrombolytic therapy. Because quantitative PET preferentially requires invasive arterial blood sampling in order to obtain an input function for kinetic CBF modeling, this procedure is not applicable in these patients. As a consequence, [^{15}O]H_2O PET did not manage to become a clinical routine imaging tool in the acute stroke situation. Clinical applications instead mainly refer to chronic cerebrovascular disorders, brain tumors, and brain activation studies. Moreover, due to the wide acceptance of PET as standard for CBF visualization and quantification, the method is used as the reference to validate other brain perfusion imaging techniques, like perfusion-weighted or arterial spin labeling MRI (Zaro-Weber et al. 2010a, b; Chen et al. 2008)

Apart from [^{15}O]H_2O PET, CBF measurements with [^{11}C]butanol have been suggested to be an alternative tracer for detection with PET. In comparison to radiolabeled water, butanol has the advantage of being permeable through the blood–brain barrier to 100 %. However, this tracer is not used in routine practice because of its complex and radiochemical synthesis (Herscovitch et al. 1987).

[^{14}C]iodoantipyrine (IAP) autoradiography is another nuclear medicine perfusion imaging method used in preclinical research (Hatakeyama et al. 1992; Jay et al. 1988). As with butanol and H_2O, IAP is also able to freely cross the blood–brain barrier. It is not metabolized and as such accumulates in the brain tissue depending on the regional CBF. After tracer application, the animals need to be sacrificed to prevent tracer diffusion and to autoradiographically determine the CBF at the time-point of tracer injection. Sequential arterial blood samples can be used for absolute CBF quantification. This autoradiographic ex vivo method provides accurate and high-resolution quantitative CBF values for a specific time-point and is therefore mainly used in small animal studies.

4.5.2.2 Computed Tomography Methods

The physical principle that underlies the CT technique is based on tissue-specific attenuation of X-rays that are directed to the body. The image contrast then resulted from variations in attenuation depending on tissue density. Due to similar densities in white and gray matter structures, this technique is not the ideal tool to image anatomical brain structures (Griffiths et al. 2001). However, with a bolus injection of a contrast agent, such as iodine, most prerequisites of the abovementioned indicator dilution theory are satisfied to measure blood flow in the brain. However, due to different acquisition hardware, acquisition protocols, varying post-processing protocols, and differences in the interpretation of perfusion CT data, a reliable CBF quantification remains challenging and varies widely between centers (Kudo et al. 2010). A further approach for CBF measurement uses inhaled Xenon to detect concentration changes of the substance (Pindzola and Yonas 1998). The lipophilic gas is soluble in water, and its X-ray attenuation is similar to that of iodine. As in ^{133}Xe SPECT, the Xe–CT technique also utilizes the Kety–Schmidt method to calculate quantitative CBF maps with sufficient accuracy (Wintermark et al. 2005). Although newer CT scanners are able to achieve whole brain coverage, a main limitation of commonly used CT scanners derives from the limited anatomical coverage, which is restricted to few brain slices.

4.5.2.3 Magnetic Resonance Methods

Several methods for CBF estimation by means of MR had been developed. The most commonly used method for neuroimaging studies is the dynamic susceptibility contrast (DSC) MRI method. It relies on changes in relaxation time on T2*-weighted images. With the bolus of a paramagnetic contrast agent agents (e.g., gadolinium-DTPA) passing through the vascular system, a detectable signal loss occurs in T2*-weighted sequences. Mathematical conclusions were then drawn from the signal reductions to further calculate several perfusion or perfusion-related parameters including mean transit time (MTT), time to peak (TTP), relative cerebral blood volume (rCBV), and relative CBF (Ostergaard et al. 1996a, b). Contrast agents for MR imaging are not radioactive and relatively inexpensive as compared with PET and SPECT tracers. A further advantage of this method is the short acquisition time that enables to visualize perfusion-weighted measurements within a few minutes. However, the absolute quantification of CBF remains unsolved (Wintermark et al. 2005). The use of a local internal input function (Calamante et al. 2004) is necessary to receive parametric maps. As such, the detection of a plausible AIF which is influenced by numerous factors, such as partial volume effects, is important for reproducible and reliable perfusion values (van Osch et al. 2001). Another respective challenge is the localization of the intracranial region of interest for the AIF calculation (Zaro-Weber et al. 2012). Thus, most of the calculated parameter maps in perfusion MR are named as "relative" (Griffiths et al. 2001; Jezzard 1998). Nevertheless, perfusion MRI is employed for diagnostic purposes, for instance in acute stroke, and in clinical settings regarding the combination of the various readout parameters. In comparison to gadolinium-based MRI, the arterial spinlabeling approach is another promising MR perfusion technique. Here, magnetically labeled water protons are used as endogenous tracer. However, problems with image interpretation may occur due to a limited signal-to-noise ratio and in the presence of prolonged blood transit times, like in patients with stroke or atherosclerosis (Petersen et al. 2006). In latter cases (e.g., stroke patients), the labeled water spins did not reach the target brain tissue within a given time, with the consequence of underestimating the real blood flow values (Jezzard 1998; Kimura et al. 2005).

4.6 Applications for CBF PET

4.6.1 Cerebral Ischemia

The increasing incidence for vascular diseases, like atherosclerosis, is associated with a worldwide increasing number of ischemic attacks (Feigin et al. 2009). Interruptions in brain–blood supply rapidly leads to ischemic cell damage that results in necrotic tissue if no sufficient therapy or spontaneous reperfusion becomes available. Current therapies aim to restore perfusion in the ischemic, salvageable brain tissue. In order to determine this hypoperfused yet viable tissue – the so-called ischemic penumbra (Astrup et al. 1981) – in acute stroke patients, perfusion imaging techniques were developed to identify this "tissue at risk" and to separate it from the already necrotic infarction core. The transition from reversible to irreversible damage is a function of ischemia duration as well as of CBF. A hemodynamic determination of the ischemic penumbra is used for many research studies in laboratory animals and humans, and CBF thresholds to characterize different tissue states were proposed: While normal human CBF is in the range of 50–80 ml/100 g/min, reversible ischemia ("ischemic penumbra") is evident when CBF drops below values around 22 ml/100 g/min, and neuronal cell death occurs below a CBF of 8 ml/100 g/m in (Baron 2001). However, penumbra detection, based on CBF thresholds, is highly dependent on a reliable and accurate quantitative imaging method in an acute stroke diagnostic setting.

The opportunity to investigate different parameters of brain function, like CBF, CBV, OEF, and $CMRO_2$, within one PET imaging session is a further advantage in the investigation of cerebrovascular diseases such as ischemic stroke. Here, it is essential to reliably separate primary perfusion deficits from events of decreased metabolic demand. This is as CBF decreases may not only appear in the surrounding tissue of the stenotic vessel, but sometimes also distant from the obviously damaged part of the brain. This well-recognized phenomenon is called "diaschisis." One example is the so-called crossed cerebellar diaschisis in which a CBF reduction in the cerebellum contralateral to the stroke-affected brain hemisphere occurs as a result of crossed functional deafferentiation (Baron et al. 1981; Feeney and Baron 1986).

4.6.1.1 PET Perfusion Imaging in Preclinical Stroke Research

This paragraph will handle the employment of $[^{15}O]H_2O$ PET in translational research studies of experimental stroke.

In 2008, our group proposed a new large animal model that is applicable for acute and chronic stroke induction (Boltze et al. 2008) and is highly suitable to reflect the human brain pathophysiology. Due to a similar cerebral anatomy and the favorable ovine brain size, brain imaging protocols, scanners, and data analysis techniques as used in clinical routine become feasible. This enables us to perform studies while meeting main conditions for translational research. Like in humans, in sheep, the middle cerebral artery (MCA) usually gives rise to three arterial branches. Different stroke sizes can be induced by permanent transcranial occlusion of one, two, or all three MCA branches, with the latter being referred to as permanent MCA occlusion (pMCAO). Fig. 4.3 shows examples of different occlusion types for experimental pMCAO in sheep. One-, two-, and three-branch (total) occlusions of the MCA could clearly be visualized by magnetic resonance angiography (MRA), together with the resulting CBF defects in $[^{15}O]H_2O$ PET. In addition, slight CBF decreases, probably due to the transcranial surgery, were also detected in the sham-operated animals. Further, it was possible to demonstrate that the ischemic strokes

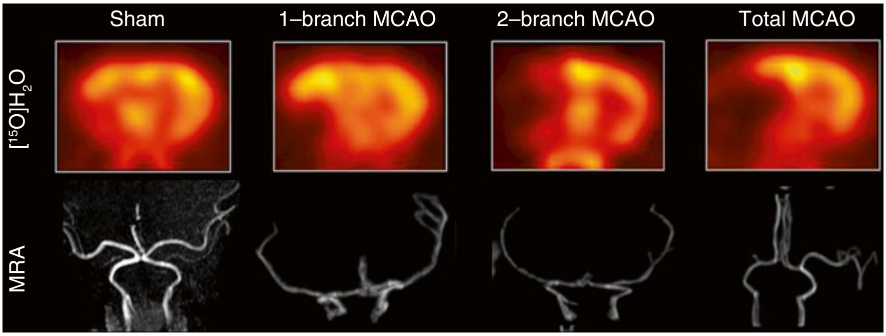

Fig. 4.3 Differential CBF deficits dependent on extent of experimental permanent middle cerebral artery occlusion in sheep. The extent of the post-pMCAO CBF deficit is clearly visualized with [^{15}O]H_2O PET. Corresponding to angiographic MRI findings, the CBF deficit increases in the order sham >1-branch pMCAO > 2-branch pMCAO > total pMCAO. *MCAO* middle cerebral artery occlusion, *MRA* magnetic resonance angiography (Modified from Boltze et al. (2008))

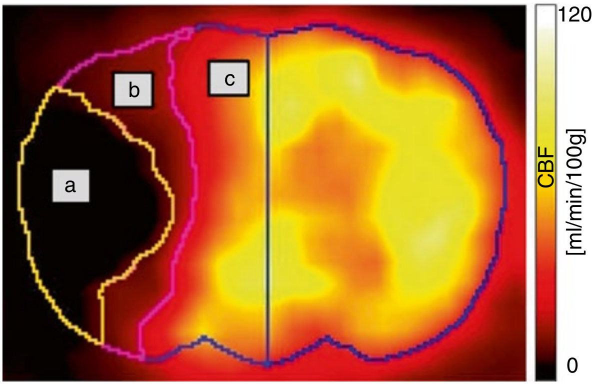

Fig. 4.4 Parametric CBF map as obtained by [^{15}O]H_2O PET in the Leipzig permanent middle cerebral artery occlusion sheep stroke model. For volume of interest analysis, the stroke-related regions were defined as follows: infarction core (**a**): <8 ml/100 g/min, ischemic penumbra: (**b**) 8–22 ml/100 g/min, normal brain tissue (**c**): >22 ml/100 g/min

induced by the transcranial pMCAO lead to reproducible CBF deficits, which remain stable over time and eventually leading to necrotic brain tissue.

The major advantage of [^{15}O]H_2O PET is the option to perform serial scans in a short time period due to the short half-life of the ^{15}O (122 s). As an example, CBF PET measurements were applied for a controlled preclinical study that aimed to test inhaled nitrous oxide (iNO) for its potential to protect the ischemic tissue in the penumbra in acute ischemic stroke. All animals were subjected to repeated PET scans at 110, 150, 175, and 210 min following pMCAO (a total of four PET scans within 100 min). In the treatment group, 50 ppm iNO were applied from 120 to 180 min after pMCAO. By using kinetic modeling, parametric CBF maps were created. Based on the abovementioned commonly accepted CBF thresholds (Baron 2001), operator-independent brain volumes of interest were defined for penumbra, infarction core, and remaining normal brain tissue (Fig. 4.4). Our experiments showed that iNO selectively restores CBF in the ischemic penumbra. While the volume of the necrotic core was not affected, the volume of the penumbra decreased by up to 50 % turning into normally perfused tissue (>22 ml/100 g/min) under iNO application, but remained unchanged in the untreated control animals ($p < 0.05$ vs. baseline and vs. control; Figs. 4.5 and 4.6; Terpolilli et al. 2012).

To give an outlook for further projects on CBF PET imaging in the Leipzig sheep pMCAO stroke model, Fig. 4.7 shows first images acquired by a simultaneous PET/3T-MRI system (Biograph mMR, Siemens). Comparative PET and MR imaging studies in acute stroke setting will greatly benefit from the new possibility to acquire data of both modalities simultaneously. This will significantly improve the investigation of the very fast pathophysiological processes in early ischemia. The first experience with this new simultaneous imaging approach, however, triggers great enthusiasm to employ this new technique for further preclinical and clinical research in the acute stroke situation.

With regard to the abovementioned possibility of PET imaging to provide multiparameter readouts (CBF, OEF, $CMRO_2$, CBV), in experimental ischemic stroke, so far mainly the brains of monkeys (Kuge et al. 2001; Pappata et al. 1993), pigs (Sakoh et al. 2000a) and felines (Heiss et al. 1994) were investigated by using [^{15}O]H_2O for CBF measurements. With examinations of different time points after stroke, the studies by Heiss et al. aimed at monitoring important parameters of the temporal transversion of penumbral tissue to the final infarct core. The ischemic penumbra is characterized by an initial increase of OEF and CBV and preserved values of $CMRO_2$. In progress of the infarct and decreasing blood flow supply, $CMRO_2$ declines to values of 25 % of baseline within the first hour after stroke, while the initially increase of OEF becomes less prominent. In the final stage, the lack of CBF

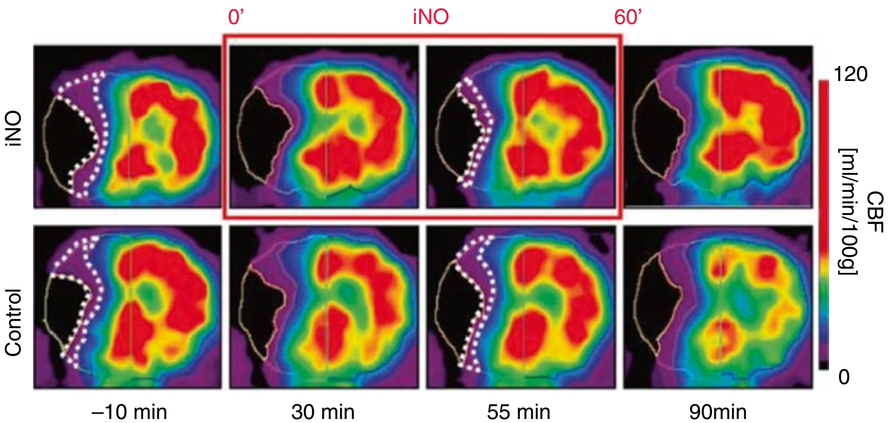

Fig. 4.5 Serial [^{15}O]H_2O PET scans show therapeutic effect of iNO in the Leipzig permanent middle cerebral artery occlusion sheep stroke model. Stroke-related tissue regions were defined on the basis of quantitative CBF maps. Volumetric analysis showed a significant decrease of the penumbra volume under iNO therapy in favor of the normal brain tissue compartment. This beneficial effect was not detected in control animals (Terpolilli et al. 2012)

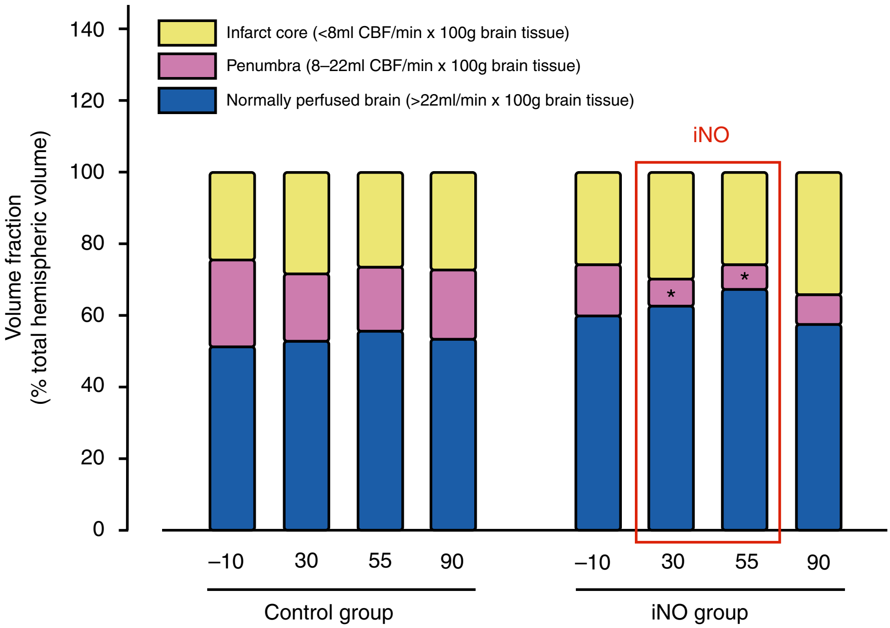

Fig. 4.6 iNO improves penumbral blood flow after permanent middle cerebral artery occlusion in sheep. Quantification of normally perfused, ischemic, and penumbral tissue volumes revealed that penumbral volume decreased significantly during NO inhalation ($n=3$ per group; $*p<0.05$ vs. control and vs. baseline PET at t-10 min) in favor of the normally perfused brain tissue (Terpolilli et al. 2012)

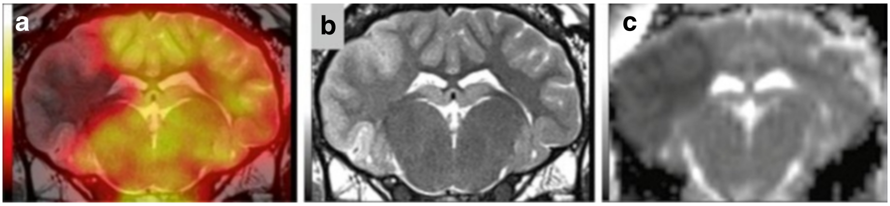

Fig. 4.7 Multimodal PET-MRI imaging in the Leipzig sheep stroke model. Four hours after permanent middle cerebral artery occlusion, (**a**) CBF was determined by $[^{15}O]H_2O$ PET (shown here in overlay with anatomical T2-MRI) demonstrating the typical poststroke deficit. (**b**) T2-MRI acquired to exclude hemorrhage. (**c**) Diffusion-weighted MRI with deficit similar to the CBF abnormality. The image data were acquired simultaneously using a PET/3T-MR (Siemens mMR) system

is associated with a decrease in OEF and the occurrence of brain tissue necrosis. This progress from still viable to necrotic tissue was defined as a function of duration and severity of stroke (Heiss et al. 1994, 1997; Heiss and Rosner 1983). In further experiments from the Cologne group, postischemic hemodynamic and metabolic processes were investigated after temporary MCAO (from 30 to 120 min of duration) in anesthetized cats (Heiss et al. 1997). CBF PET was performed immediately after MCAO and was repeated at 30-min intervals. After reopening the vessel, a distinct hyperperfusion was found in all animals, depending on the duration of the MCAO. After 30 min of ischemia, the reactive CBF increase was found to be transient with a fast normalization to pre-occlusion CBF values and without major tissue necrosis. By comparison, the reperfusion period after 60 or 120 min of ischemia was associated with severe hyperperfusion (CBF increase up to 300 % compared to basal levels) and irreversible tissue damage, depending on the severity of prior ischemia. Approximately 50 % of animals died after the prolonged ischemic period and suffered from higher CBF than the surviving animals from the same group. One explanation might be the hyperperfusion processes with massive cerebral edema that resulted in malignant brain swelling. These observations let to assume a relatively high tolerance against moderate hyperemia, whereas extensive hyperperfusion leads to an increased mortality (Heiss et al. 1997).

Other large animal experiments utilized $[^{15}O]H_2O$ (Sakoh et al. 2000a, b) in combination with $[^{15}O]CO$ PET to study regional correlations of CBF and CBV after acute stroke and in cases of reperfusion (Sakoh et al. 2000a). For that purpose, 13 pigs underwent PET, and the results were compared to MRI measurements of the same parameters. A good agreement was found between the values of both modalities in the ischemic tissue. After MCAO, a significant correlation between CBF reduction and CBV increase was observed. However, the decrease of CBF below 60 % of the contralateral side was found to induce a reduction in CBV. In contrast, both parameters were less correlated in cases of reperfusion (Sakoh et al. 2000a).

4.6.2 Activation Studies

Perfusion parameters are closely coupled with changes in neuronal activity (Roy and Sherrington 1890; Fox et al. 1988; Villringer and Dirnagl 1995). In the last decades, numerous neuronal activation studies have reported this effect, which, nevertheless, is not completely understood (Peterson et al. 2011). The possibility to perform sequential measurements within a certain time window made CBF PET an attractive tool to study perfusion during cognitive, motor, or sensomotor tasks in humans. During local brain activation, cerebral areas that are involved in task performance were identified by CBF changes (Feng et al. 2004; Worsley et al. 1992).

4.6.3 Other Applications for CBF PET

In general, PET is a useful tool to study perfusion and oxygen metabolism in any cerebral disease, such as dementia (Yao et al. 1990; Cohen et al. 1997), schizophrenia (Ragland et al. 2001), and migraine. Latter approaches addressed hemodynamic changes and oxygen metabolism during and between acute attacks. An increase in CBF was found in cortical areas and in the brainstem which appeared to be pain related (Andersson et al. 1997; Cutrer et al. 2000). Similar to these migraine studies, other preclinical and clinical investigations focus on epilepsy to determine perfusion changes during and between epileptic seizures (Szabo et al. 2007; Kahane 1999; Gaillard et al. 1995). A few studies also used CBF PET (mostly in combination with other PET readouts, like oxygen metabolism from ^{15}O inhalation) for detailed characterization of brain tumors (Leenders 1994; Hino et al. 1990; Tomura et al. 1993). Due to the neo-formed vessels which often appear in the tumor parenchyma or its surrounding, a regional CBF increase could be detected and may provide additionally useful information about the progression of the brain tumors.

4.7 Summary and Conclusions

PET imaging with $[^{15}O]H_2O$ represents the gold standard to visualize and quantify CBF in vivo. As such, this method plays a relevant role mainly for the investigation of cerebrovascular diseases. Despite advantageous characteristics of the tracer, like the possibility to monitor CBF changes over time in sequential scans, $[^{15}O]H_2O$ PET imaging remains a technological and infrastructural challenge, preventing it from gaining a wider acceptance in a clinical routine setting. In contrast to clinical routine, $[^{15}O]H_2O$ PET plays an important role in preclinical and clinical research, for instance, in (1) clarifying the pathophysiology of ischemic stroke and other cerebrovascular disorders, (2) cross-evaluation of alternative imaging methods to estimate CBF, and (3) the testing of new stroke treatment concepts.

Acknowledgments The authors are grateful to the cyclotron, radiochemistry, and PET crews of the Department of Nuclear Medicine of the Leipzig University Hospital for their excellent support in acquiring the PET data. Further, we would like to thank the stroke sheep model group of the Leipzig Fraunhofer Institute for Cell Therapy and Immunology for providing the research animals, and to our collaborators at the Department of Neuroradiology of the Leipzig University Hospital for providing the sheep MRI data.

References

Andersson JL, Muhr C, Lilja A et al (1997) Regional cerebral blood flow and oxygen metabolism during migraine with and without aura. Cephalalgia 17(5):570–579

Astrup J, Siesjö BK, Symon L (1981) Thresholds in cerebral ischemia – the ischemic penumbra. Stroke 12(6):723–725

Baron JC (2001) Perfusion thresholds in human cerebral ischemia: historical perspective and therapeutic implications. Cerebrovasc Dis 11 Suppl 1:2–8

Baron JC, Bousser MG, Comar D et al (1981) “Crossed cerebellar diaschisis” in human supratentorial brain infarction. Trans Am Neurol Assoc 105:459–461

Barthel H, Hesse S, Dannenberg C et al (2001) Prospective value of perfusion and X-ray attenuation imaging with single-photon emission and transmission computed tomography in acute cerebral ischemia. Stroke 32(7):1588–1597

Beaver J, Finn RD, Hupf HB et al (1976) A new method for the production of high concentration oxygen-15 labeled carbon dioxide with protons. Appl Radiat Isot 27:195–197

Berridge MS, Terries AH, Cassidy EH et al (1990) Low-carrier production of [15O]oxygen, water and carbon monoxide. Appl Radiat Isot 41:1173–1175

Boltze J, Forschler A, Nitzsche B et al (2008) Permanent middle cerebral artery occlusion in sheep: a novel large animal model of focal cerebral ischemia. J Cereb Blood Flow Metab 28(12):1951–1964

Bolwig TG, Lassen NA (1975) The diffusion permeability to water of the rat blood–brain barrier. Acta Physiol Scand 93(3):415–422
Brody H (1955) Organization of the cerebral cortex. III. A study of aging in the human cerebral cortex. J Comp Neurol 102(2):511–516
Bruce DA, Langfitt TW, Miller JD et al (1973) Regional cerebral blood flow, intracranial pressure, and brain metabolism in comatose patients. J Neurosurg 38(2):131–144
Calamante F, Morup M, Hansen LK (2004) Defining a local arterial input function for perfusion MRI using independent component analysis. Magn Reson Med 52(4):789–797
Carroll TJ, Teneggi V, Jobin M et al (2002) Absolute quantification of cerebral blood flow with magnetic resonance, reproducibility of the method, and comparison with H215O positron emission tomography. J Cereb Blood Flow Metab 22:1149–1156
Chen JJ, Wieckowska M, Meyer E et al (2008) Cerebral blood flow measurement using fMRI and PET: a cross-validation study. Int J Biomed Imaging 2008:516359
Chiron C, Raynaud C, Maziere B et al (1992) Changes in regional cerebral blood flow during brain maturation in children and adolescents. J Nucl Med 33(5):696–703
Clark JC, Crouzel C, Meyer GJ et al (1987) Current methodology for oxygen-15 production for clinical use. Int J Rad Appl Instrum A 38(8):597–600
Clark JC, Tochon-Danguy H (1991) R2D2, - a bedside [oxygen-15]water infuser. PSI Proceedings 92-01, pp 234–235. ISSN 1019-6447. Proc. IV. Int. Workshop on Targetry and Target Chemistry; Sept 9-12th; Villigen, Switzerland, 1991. (Abstract)
Cohen RM, Andreason PJ, Doudet DJ et al (1997) Opiate receptor avidity and cerebral blood flow in Alzheimer's disease. J Neurol Sci 148(2):171–180
Cutrer FM, O'Donnell A, Sanchez del Rio M (2000) Functional neuroimaging: enhanced understanding of migraine pathophysiology. Neurology 55(9 Suppl 2):S36–S45
Eichling JO, Raichle ME, Grubb RL et al (1974) Evidence of the limitations of water as a freely diffusible tracer in brain of the rhesus monkey. Circ Res 35(3):358–364
Feeney DM, Baron JC (1986) Diaschisis. Stroke 17(5):817–830
Feigin VL, Lawes CMM, Bennett DA et al (2009) Worldwide stroke incidence and early case fatality reported in 56 population-based studies: a systematic review. Lancet Neurol 8(4):355–369
Feng C, Narayana S, Lancaster JL et al (2004) CBF changes during brain activation: fMRI vs. PET. Neuroimage 22(1):443–446
Fox PT, Mintun MA, Reiman EM et al (1988) Enhanced detection of focal brain responses using intersubject averaging and change-distribution analysis of subtracted PET images. J Cereb Blood Flow Metab 8(5):642–653
Frackowiak RS, Lenzi GL, Jones T et al (1980) Quantitative measurement of regional cerebral blood flow and oxygen metabolism in man using 15O and positron emission tomography: theory, procedure, and normal values. J Comput Assist Tomogr 4(6):727–736
Gaillard WD, Fazilat S, White S et al (1995) Interictal metabolism and blood flow are uncoupled in temporal lobe cortex of patients with complex partial epilepsy. Neurology 45(10): 1841–1847
Griffiths PD, Hoggard N, Dannels WR et al (2001) In vivo measurement of cerebral blood flow: a review of methods and applications. Vasc Med 6(1):51–60
Hall R (1971) Vascular injuries resulting from arterial puncture of catheterization. Br J Surg 58(7): 513–516
Hatakeyama T, Sakaki S, Nakamura K et al (1992) Improvement in local cerebral blood flow measurement in gerbil brains by prevention of postmortem diffusion of 14Ciodoantipyrine. J Cereb Blood Flow Metab 12(2):296–300
Heiss WD, Rosner G (1983) Functional recovery of cortical neurons as related to degree and duration of ischemia. Ann Neurol 14(3):294–301
Heiss WD, Graf R, Wienhard K et al (1994) Dynamic penumbra demonstrated by sequential multitracer PET after middle cerebral artery occlusion in cats. J Cereb Blood Flow Metab 14(6):892–902
Heiss WD, Graf R, Lottgen J et al (1997) Repeat positron emission tomographic studies in transient middle cerebral artery occlusion in cats: residual perfusion and efficacy of postischemic reperfusion. J Cereb Blood Flow Metab 17(4):388–400

Heiss W, Kracht L, Grond M et al (2000) Early [11C]flumazenil/H2O positron emission tomography predicts irreversible ischemic cortical damage in stroke patients receiving acute thrombolytic therapy. Stroke 31(2):366–369

Herscovitch P, Raichle ME (1985) What is the correct value for the brain–blood partition coefficient for water? J Cereb Blood Flow Metab 5(1):65–69

Herscovitch P, Raichle ME, Kilbourn MR et al (1987) Positron emission tomographic measurement of cerebral blood flow and permeability-surface area product of water using 15Owater and 11Cbutanol. J Cereb Blood Flow Metab 7(5):527–542

Hino A, Imahori Y, Tenjin H et al (1990) Metabolic and hemodynamic aspects of peritumoral low-density areas in human brain tumor. Neurosurgery 26(4):615–621

Hoeffner EG (2005) Cerebral perfusion imaging. J Neuroophthalmol 25(4):313–320

Ibaraki M, Shimosegawa E, Miura S et al (2004) PET measurements of CBF, OEF, and CMRO2 without arterial sampling in hyperacute ischemic stroke: method and error analysis. Ann Nucl Med 18(1):35–44

Iida H, Jones T, Miura S (1993) Modeling approach to eliminate the need to separate arterial plasma in oxygen-15 inhalation positron emission tomography. J Nucl Med 34(8):1333–1340

Jay TM, Lucignani G, Crane AM et al (1988) Measurement of local cerebral blood flow with [14C] iodoantipyrine in the mouse. J Cereb Blood Flow Metab 8(1):121–129

Jezzard P (1998) Advances in perfusion MR imaging. Radiology 208(2):296–299

Kahane P (1999) An H215O-PET study of cerebral blood flow changes during focal epileptic discharges induced by intracerebral electrical stimulation. Brain 122(10):1851–1865

Kanno I, Iida H, Miura S et al (1991) Optimal scan time of oxygen-15-labeled water injection method for measurement of cerebral blood flow. J Nucl Med 32(10):1931–1934

Kety SS, Schmidt CF (1945) The determination of cerebral blood flow in man by use of nitrous oxide in low concentrations. Am J Physiol 143:53–66

Kety SS (1951) The theory and applications of the exchange of inert gas at the lungs and tissues. Pharmacol Rev 3:1–41

Kimura H, Kado H, Koshimoto Y et al (2005) Multislice continuous arterial spin-labeled perfusion MRI in patients with chronic occlusive cerebrovascular disease: a correlative study with CO2 PET validation. J Magn Reson Imaging 22(2):189–198

Krohn K, Link JM, Lewellen TK et al (1986) The use of 50 MeV protons to produce C-11 and O-15. J Labelled Compd Radiopharm 23:1190–1192

Kudo K, Sasaki M, Yamada K et al (2010) Differences in CT perfusion maps generated by different commercial software: quantitative analysis by using identical source data of acute stroke patients. Radiology 254(1):200–209

Kuge Y, Yokota C, Tagaya M et al (2001) Serial changes in cerebral blood flow and flow-metabolism uncoupling in primates with acute thromboembolic stroke. J Cereb Blood Flow Metab 21(3):202–210

Lammertsma AA (1994) Noninvasive estimation of cerebral blood flow. J Nucl Med 35(11):1878–1879

Lass P, Koseda M, Romanowicz G et al (1998) Cerebral blood flow assessed by brain SPECT with 99mTc-HMPAO utilising the acetazolamide test in systemic lupus erythematosus. Nucl Med Rev Cent East Eur 1(1):20–24

Lassen NA, Ingvar DH (1961) The blood flow of the cerebral cortex determined by radioactive krypton. Experientia 17:42–43

Law I, Iida H, Holm S et al (2000) Quantitation of regional cerebral blood flow corrected for partial volume effect using O-15 water and PET: II. Normal values and gray matter blood flow response to visual activation. J Cereb Blood Flow Metab 20(8):1252–1263

Leenders KL (1994) PET: blood flow and oxygen consumption in brain tumors. J Neurooncol 22(3):269–273

Links JM, Zubieta JK, Meltzer CC et al (1996) Influence of spatially heterogeneous background activity on "hot object" quantitation in brain emission computed tomography. J Comput Assist Tomogr 20(4):680–687

Machleder HI, Sweeney JP, Barker WF (1972) Pulseless arm after brachial-artery catheterisation. Lancet 1(7747):407–409

Markus HS (2004) Cerebral perfusion and stroke. J Neurol Neurosurg Psychiatry 75(3):353–361
Martin WR, Powers WJ, Raichle ME (1987) Cerebral blood volume measured with inhaled C15O and positron emission tomography. J Cereb Blood Flow Metab 7(4):421–426
Matsuda M, Lee H, Kuribayashi K et al (1996) Comparative study of regional cerebral blood flow values measured by Xe CT and Xe SPECT. Acta Neurol Scand Suppl 166:13–16
Matthew E, Andreason P, Carson RE et al (1993) Reproducibility of resting cerebral blood flow measurements with H2(15)O positron emission tomography in humans. J Cereb Blood Flow Metab 13(5):748–754
Meier P, Zierler KL (1954) On the theory of the indicator-dilution method for measurement of blood flow and volume. J Appl Physiol 6(12):731–744
Mulholland GK, Kilbourn MR, Moskwa JJ (1990) Direct simultaneous production of 15Owater and 13Nammonia or 18Ffluoride ion by 26 MeV proton irradiation of a double chamber water target. Int J Rad Appl Instrum A 41(12):1193–1199
Obrist WD, Thompson HK JR, Wang HS et al (1975) Regional cerebral blood flow estimated by 133-xenon inhalation. Stroke 6(3):245–256
Ostergaard L, Weisskoff RM, Chesler DA et al (1996a) High resolution measurement of cerebral blood flow using intravascular tracer bolus passages. Part I: mathematical approach and statistical analysis. Magn Reson Med 36(5):715–725
Ostergaard L, Sorensen AG, Kwong KK et al (1996b) High resolution measurement of cerebral blood flow using intravascular tracer bolus passages. Part II: experimental comparison and preliminary results. Magn Reson Med 36(5):726–736
Pantano P, Baron JC, Lebrun-Grandie P et al (1984) Regional cerebral blood flow and oxygen consumption in human aging. Stroke 15(4):635–641
Pappata S, Fiorelli M, Rommel T et al (1993) PET study of changes in local brain hemodynamics and oxygen metabolism after unilateral middle cerebral artery occlusion in baboons. J Cereb Blood Flow Metab 13(3):416–424
Petersen ET, Zimine I, Ho YL et al (2006) Non-invasive measurement of perfusion: a critical review of arterial spin labelling techniques. Br J Radiol 79(944):688–701
Peterson EC, Wang Z, Britz G (2011) Regulation of cerebral blood flow. Int J Vasc Med 2011:1–8
Pindzola RR, Yonas H (1998) The xenon-enhanced computed tomography cerebral blood flow method. Neurosurgery 43(6):1488–1492
Powell J, O'Neil JP (2006) Production of 15Owater at low-energy proton cyclotrons. Appl Radiat Isot 64(7):755–759
Ragland JD, Gur RC, Raz J, et al (2001) Effect of schizophrenia on frontotemporal activity during word encoding and recognition: a PET cerebral blood flow study. Am J Psychiatry 158(7):1114–1125
Raichle ME, Martin WR, Herscovitch P et al (1983) Brain blood flow measured with intravenous H2(15)O. II. Implementation and validation. J Nucl Med 24(9):790–798
Rousset OG, Ma Y, Evans AC (1998) Correction for partial volume effects in PET: principle and validation. J Nucl Med 39(5):904–911
Roy CS, Sherrington CS (1890) On the regulation of the blood-supply of the brain. J Physiol 11(1–2):85–158
Sajjad M, Liow JS, Moreno-Cantu J (2000) A system for continuous production and infusion of 15OH2O for PET activation studies. Appl Radiat Isot 52(2):205–210
Sakoh M, Rohl L, Gyldensted C et al (2000a) Cerebral blood flow and blood volume measured by magnetic resonance imaging bolus tracking after acute stroke in pigs: comparison with [15O] H2O positron emission tomography. Stroke 31(8):1958–1964
Sakoh M, Ostergaard L, Røhl L et al (2000b) Relationship between residual cerebral blood flow and oxygen metabolism as predictive of ischemic tissue viability: sequential multitracer positron emission tomography scanning of middle cerebral artery occlusion during the critical first 6 hours after stroke in pigs. J Neurosurg 93(4):647–657
Sakai Y, Kasuga T, Nakanishi F et al (1987) Cerebral blood flow study by 133Xe inhalation and single photon emission CT in occlusive cerebrovascular diseases. Kaku Igaku 24(1):47–54

Skyhøj Olsen T, Larsen B, Bech Skriver E et al (1981) Focal cerebral ischemia measured by the intra-arterial 133xenon method. Limitations of 2-dimensional blood flow measurements. Stroke 12(6):736–744

Slosman DO, Chicherio C, Ludwig C et al (2001) (133)Xe SPECT cerebral blood flow study in a healthy population: determination of T-scores. J Nucl Med 42(6):864–870

Sokoloff L, Perlin S, Kornetsky C et al (1957) The effects of D-lysergic acid diethylamide on cerebral circulation and overall metabolism. Ann N Y Acad Sci 66(3):468–477

Szabo CA, Narayana S, Kochunov PV et al (2007) PET imaging in the photosensitive baboon: case-controlled study. Epilepsia 48(2):245–253

Tomura N, Kato T, Kanno I et al (1993) Increased blood flow in human brain tumor after administration of angiotensin II: demonstration by PET. Comput Med Imaging Graph 17(6):443–449

Terpolilli NA, Kim S, Thal SC et al (2012) Inhalation of nitric oxide prevents ischemic brain damage in experimental stroke by selective dilatation of collateral arterioles. Circ Res 110(5):727–738

van Naemen J, Monclus M, Damhaut P et al (1996) Production, automatic delivery and bolus injection of 15Owater for positron emission tomography studies. Nucl Med Biol 23(4):413–416

van Osch MJ, Vonken EJ, Bakker CJ et al (2001) Correcting partial volume artifacts of the arterial input function in quantitative cerebral perfusion MRI. Magn Reson Med 45(3):477–485

Veall N, Mallett BL (1967) The Xe133 inhalation technique for regional cerebral blood flow studies. Strahlentherapie Sonderb 65:166–173

Villringer A, Dirnagl U (1995) Coupling of brain activity and cerebral blood flow: basis of functional neuroimaging. Cerebrovasc Brain Metab Rev 7(3):240–276

Wakita K, Imahori Y, Ido T et al (2000) Simplification for measuring input function of FDG PET: investigation of 1-point blood sampling method. J Nucl Med 41(9):1484–1490

Watabe H, Itoh M, Cunningham V et al (1996) Noninvasive quantification of rCBF using positron emission tomography. J Cereb Blood Flow Metab 16:311–319

Wintermark M, Sesay M, Barbier E et al (2005) Comparative overview of brain perfusion imaging techniques. J Neuroradiol 32(5):294–314

Worsley KJ, Evans AC, Marrett S et al (1992) A three-dimensional statistical analysis for CBF activation studies in human brain. J Cereb Blood Flow Metab 12(6):900–918

Yao H, Sadoshima S, Kuwabara Y et al (1990) Cerebral blood flow and oxygen metabolism in patients with vascular dementia of the Binswanger type. Stroke 21(12):1694–1699

Zanotti-Fregonara P, Chen K, Liow J et al (2011) Image-derived input function for brain PET studies: many challenges and few opportunities. J Cereb Blood Flow Metab 31(10):1986–1998

Zaro-Weber O, Moeller-Hartmann W, Heiss W et al (2010a) Maps of time to maximum and time to peak for mismatch definition in clinical stroke studies validated with positron emission tomography. Stroke 41(12):2817–2821

Zaro-Weber O, Moeller-Hartmann W, Heiss W et al (2010b) MRI perfusion maps in acute stroke validated with 15O-water positron emission tomography. Stroke 41(3):443–449

Zaro-Weber O, Moeller-Hartmann W, Heiss W et al (2012) Influence of the arterial input function on absolute and relative perfusion-weighted imaging penumbral flow detection: a validation with ^{15}O-water positron emission tomography. Stroke 43(2):378–385

Zierler K (1962) Theoretical basis of indicator-dilution methods for measuring flow and volume. Circ Res 10:393–407